Biochimica et Biophysica Acta 1828 (2013) 2419–2427

Contents lists available at ScienceDirect

Biochimica et Biophysica Acta

journal homepage: www.elsevier.com/locate/bbamem

$rBPI_{21}$ interacts with negative membranes endothermically promoting the formation of rigid multilamellar structures

Marco M. Domingues [a], M. Lucia Bianconi [b], Leandro R.S. Barbosa [c], Patrícia S. Santiago [d,e], Marcel Tabak [d], Miguel A.R.B. Castanho [a], Rosangela Itri [c], Nuno. C. Santos [a,*]

[a] Instituto de Medicina Molecular, Faculdade de Medicina, Universidade de Lisboa, Av. Prof. Egas Moniz, 1649-028 Lisbon, Portugal
[b] Programa de Biologia Estrutural, Instituto de Bioquímica Médica, Universidade Federal do Rio de Janeiro, Rio de Janeiro, RJ, Brazil
[c] Instituto de Física da Universidade de São Paulo, São Paulo, Brazil
[d] Instituto de Química de São Carlos, Universidade de São Paulo, São Carlos, SP, Brazil
[e] Universidade Estadual Paulista "Júlio de Mesquita Filho", Registro, SP, Brazil

ARTICLE INFO

Article history:
Received 15 November 2012
Received in revised form 30 May 2013
Accepted 10 June 2013
Available online 18 June 2013

Keywords:
Lipopolysaccharide
AMP
$rBPI_{21}$
Membrane binding
Microcalorimetry
SAXS

ABSTRACT

$rBPI_{21}$ belongs to the antimicrobial peptide and protein (AMP) family. It has high affinity for lipopolysaccharide (LPS), acting mainly against Gram-negative bacteria. This work intends to elucidate the mechanism of action of $rBPI_{21}$ at the membrane level. Using isothermal titration calorimetry, we observed that $rBPI_{21}$ interaction occurs only with negatively charged membranes (mimicking bacterial membranes) and is entropically driven. Differential scanning calorimetry shows that membrane interaction with $rBPI_{21}$ is followed by an increase of rigidity on negatively charged membrane, which is corroborated by small angle X-ray scattering (SAXS). Additionally, SAXS data reveal that $rBPI_{21}$ promotes the multilamellarization of negatively charged membranes. The results support the proposed model for $rBPI_{21}$ action: first it may interact with LPS at the bacterial surface. This entropic interaction could cause the release of ions that maintain the packed structure of LPS, ensuring peptide penetration. Then, $rBPI_{21}$ may interact with the negatively charged leaflets of the outer and inner membranes, promoting the interaction between the two bacterial membranes, ultimately leading to cell death.

1. Introduction

Bacterial resistance is considered by the World Health Organization as "a major concern because a resistant infection may kill, can spread to others, and imposes huge costs to individuals and society" [1]. Antimicrobial peptides and proteins (AMPs) are part of the innate immune system and a good alternative to conventional therapies [2–4]. They are also a good approach to overcome bacterial resistance, due to the lower opposition of bacteria against AMP mechanisms of action at the membrane level [4]. Most AMPs possess a positive net charge, which ensures the interaction with the negatively charged bacterial surface. Bacterial membranes present high percentages of negatively charged phospholipids [5–7]. In both Gram-positive and Gram-negative bacteria, the major phospholipid components are phosphatidylethanolamine (POPE), phosphatidylglycerol (POPG; negatively charged) and cardiolipin (CL) [5,6].

$rBPI_{21}$ is a protein fragment of 21 kDa, corresponding to the N-terminal 193 amino acid residues of the bactericidal/permeability-increasing protein (BPI), with a C132A point mutation [8]. This molecule revealed bactericidal effects, mainly against Gram-negative bacteria, together with lipopolysaccharide (LPS) neutralization [9,10]. LPS, a negatively charged molecule present in the outer leaflet of the outer membrane of Gram-negative bacteria, is responsible for severe health conditions. When an infection occurs, Gram-negative bacteria release LPS aggregates into the bloodstream. It interacts preferentially with monocytes and macrophages, promoting the release of cytokines [11,12]. The overproduction of these cytokines has several harmful effects, associated with septicemia and with lethal septic shock [13]. Thus, it is necessary to find new antibiotics that exert cytotoxic effects on bacteria and, at the same time, possess LPS-neutralization properties. Due to its higher affinity for LPS and consequent neutralization, together with its bactericidal effects, $rBPI_{21}$ has shown encouraging clinical benefits in severe forms of sepsis, including meningococcal septic shock [14].

Some studies of the interaction between $rBPI_{21}$ and membranes have been reported [15–18], most of them focused on its interaction with lipid membranes of different compositions, but little was shown

Abbreviations: AMPs, antimicrobial peptide and proteins; BPI, bactericidal/permeability-increasing protein; DSC, differential scanning calorimetry; ITC, isothermal titration calorimetry; LPS, lipopolysaccharide; LUV, large unilamellar vesicles; MCT, Modified Caillé Theory; MLV, multilamellar vesicles; SAXS, small angle X-ray scattering

* Corresponding author at: Unidade de Biomembranas, Instituto de Medicina Molecular, Faculdade de Medicina, Universidade de Lisboa, Av. Prof. Egas Moniz, 1649-028 Lisbon, Portugal. Tel.: +351 217999480; fax: +351 217999477.
E-mail address: nsantos@fm.ul.pt (N.C. Santos).

0005-2736/$ – see front matter © 2013 Elsevier B.V. All rights reserved.
http://dx.doi.org/10.1016/j.bbamem.2013.06.009

on the structure of the membrane and on which membrane properties are affected, leading to a high instability that culminates in its rupture, as measured by membrane leakage experiments [15]. In order to overcome the lack of information at this level, in the present study we used small angle X-ray scattering (SAXS) and differential scanning calorimetry (DSC) to evaluate the properties of membranes affected by the presence of the peptide. Additionally, isothermal titration calorimetry (ITC) was used to evaluate the preference of the peptide for biomembrane model systems with different compositions. The results obtained reinforce a hypothetical model for the mechanism of action of $rBPI_{21}$ at the molecular level previously proposed by some of us [15].

2. Materials and methods

2.1. Large unilamellar vesicles and lipopolysaccharide aggregates preparation

For the SAXS and ITC measurements, large unilamellar vesicles (LUV) with ~100 nm diameter were obtained by extrusion of multilamellar vesicles (MLV) [19]. Briefly, the lipids were dissolved in chloroform and dried under nitrogen flux in a round bottom flask. The flasks were dried overnight in vacuum, to remove any remaining traces of chloroform. Then, the lipid film was hydrated with buffer and subjected to several freeze and thaw (above the lipids phase transition temperatures) cycles. After complete hydration, the lipid suspension was extruded by passing it several times through filters with 100 nm pore size. For DSC measurements, MLV were used instead of LUV. 1,2-dipalmitoyl-*sn*-glycero-3-phospho-(1′-*rac*-glycerol) (DPPG), 1,2-dipalmitoyl-*sn*-glycero-3-phosphocholine (DPPC), 1-palmitoyl-2-oleoyl-*sn*-glycero-3-phosphocholine (POPC) and 1-palmitoyl-2-oleoyl-*sn*-glycero-3-phospho-(1′-*sn*-glycerol) (POPG) were obtained from Avanti Polar Lipids (Alabaster, AL). LPS from *Escherichia coli* (serotype O26:B6), with a molecular mass of 13 kDa, as determined by Mangoni et al. [20], was from Sigma-Aldrich (St. Louis, MO). The LUV studied were either zwitterionic (pure POPC) or anionic (POPC:POPG 80:20, 70:30, 55:45 or 30:70, w:w). Stock solutions of LPS aggregates were bath sonicated at 40 °C, during 20 min, and kept at 4 °C overnight before measurements.

2.2. Isothermal titration calorimetry

All measurements were carried out in a Microcal VP-ITC microcalorimeter (Microcal Inc./GE Healthcare Bio-Sciences, Northampton, MA, USA). The VP-ITC was electrically calibrated by the manufacturer. Peptide and lipid solutions in 20 mM Tris–HCl buffer pH 7.4, containing 150 mM NaCl, were degassed under vacuum and thermostatized at different temperatures (5, 15, and 25 °C) before measurement. The reference power was set to 20 μcal/s, using a syringe stirring speed of 242 rpm. The heat of dilution for successive injections of the lipid suspension into Tris–HCl buffer was insignificant as compared to that of peptide–lipid reaction. Although the dilution heat was negligible, it was included in the final analysis. The lipid concentration was 5 mM for all lipid systems used, with the exception of 1 mM for POPC:POPG 30:70. The $rBPI_{21}$ concentration in the reaction cell was 5 μM. The heat developed from successive injections of the lipid was determined by integrating the area under each titration peak, using the Origin software provided by the manufacturer. Under the assumption of a one-site binding model [21], with the ligand in the sample cell, the variations of the thermodynamic parameters enthalpy (ΔH) and entropy (ΔS) were calculated, as well as the equilibrium dissociation constant (K_D). Due to data signal-to-noise ratio limitations, it could not be successfully fitted with the model derived to quantify membrane partition [22,23].

2.3. Differential scanning calorimetry

All measurements were carried out with a Microcal VP-DSC calorimeter (Microcal Inc./GE Healthcare Bio-Sciences, Nothampton, MA, USA). MLV were used for these experiments. Both DPPC and DPPG were dissolved in a $CHCl_3$:CH_3OH 2:1 (v:v) mixture. The solutions of DPPC and DPPC:DPPG 55:45 were dried under a stream of nitrogen and then under high vacuum overnight. Tris–HCl buffer alone or with different $rBPI_{21}$ concentrations (5, 10, and 20 μM) was added to each sample, during the hydration process, and vortexed. The final concentration of the lipid suspensions was 2 mM. Suspensions were degassed under vacuum for 10 min before the DSC measurements. A total of 8 scans were measured for each membrane composition at a scan rate of 10 °C/h. Data acquisition and analysis were done using the Origin software.

2.4. Small angle X-ray scattering

SAXS measurements were performed with 5 mM POPC or POPC:POPG (80:20 or 55:45) in 20 mM sodium phosphate buffer, pH 7.4, containing 150 mM NaCl. These suspensions were incubated for 10 min in the absence and presence of three concentrations of $rBPI_{21}$ (5 μM, 10 μM and 20 μM). SAXS experiments were performed at the National Synchrotron Light Laboratory (LNLS), Campinas, Brazil, using a detector-to-sample distance of ~950 mm. The scattering vector amplitude, q, defined as $q = \frac{4\pi \sin\theta}{\lambda}$ (2θ being the scattering angle and λ the X-ray wavelength of 1.488 Å), ranged from $q_{min} = 0.02$ Å^{-1} to $q_{max} = 0.33$ Å^{-1}. The experimental intensities were corrected for background, buffer contributions, sample's attenuation and detector homogeneity. SAXS measurements from $rBPI_{21}$ up to 20 μM in buffer solution resulted in no detectable signal.

As it will be shown in the Results and discussion, the presence of $rBPI_{21}$ induces the formation of some MLV coexisting in solution with LUV. Thus, the SAXS intensity $I(q)$ can be written as:

$$I(q) = k(w_1 P(q) S(q) + w_2 P(q)) \quad (1)$$

where k is related to the experimental setup, and w_i is the weight of each contribution (MLV or LUV) on $I(q)$. $P(q)$ corresponds to the unilamellar vesicle form factor, such that [24–26]:

$$P(q) = \frac{2\pi A}{q^2} P_t(q) \quad (2)$$

where A is the area of the basal plane and $P_t(q)$ is the form factor of the bilayer cross-section (perpendicular to the basal plane) considered to be much smaller than the size of plane A [24]. $P_t(q)$ is thus known as the cross-section form factor, and it can be modeled by assuming that the membrane is composed by three layers of different electron densities in respect to the solvent ($\rho_{sol} = 0.33$ e/Å^3 for aqueous solution), namely: polar headgroup, with thickness R_{pol} and electron density ρ_{pol}, paraffinic chains, with length R_{par} and electron density ρ_{par}, and the methyl chain with R_{CH3} and ρ_{CH_3} [27]. This way, $P_t(q)$ is written as:

$$P_t(q) = \left\{ \frac{2}{q} \left\{ \Delta\rho_{CH_3} \sin qR_{CH_3} + \Delta\rho_{par} \left[\sin q\left(R_{par} + R_{CH_3}\right) - \sin qR_{CH_3} \right] + \Delta\rho_{pol} \left[\sin q\left(R_{pol} + R_{par} + R_{CH_3}\right) - \sin q\left(R_{par} + R_{CH_3}\right) \right] \right\} \right\}^2 \quad (3)$$

with $\Delta\rho_{CH_3} = \rho_{CH_3} - \rho_{sol}$, $\Delta\rho_{pol} = \rho_{pol} - \rho_{sol}$ and $\Delta\rho_{par} = \rho_{par} - \rho_{sol}$. The lipid bilayer thickness is, thus, $2(R_{pol} + R_{par} + R_{CH3})$. During the fitting procedure, some of these parameters were allowed to vary within a narrow range: R_{CH3} (2.0 Å < R_{CH3} < 3.5 Å), ρ_{CH_3} (0.15 e/Å^3 < ρ_{CH_3} < 0.20 e/Å^3) and ρ_{par} (0.25 e/Å^3 < ρ_{par} < 0.30 e/Å^3), in accordance with data from the literature [27]. The other $P_t(q)$ parameters were allowed to vary in a corresponding broader range.

In Eq. (1), $S(q)$ is the so-called "measured" structure factor, which is equal to 1 for non-interacting systems. In the case of multilamellar stacking of bilayers, we made use of the well-known Modified Caillé Theory (MCT) [24,28–30], which accounts for the fluctuation of the

multilamellar stacking of bilayers through a disorder parameter, $\eta_{Caillé}$ [24,29,30]. Note that $\eta_{Caillé}$ is related to the mean fluctuation of the lipid membrane such that [30]:

$$S(q) = N + 2\sum_{n=1}^{N-1}(N-n)\cos(qnD)e^{\frac{-n\left(q\sigma_{Caillé}\right)^2}{2}} \quad (4)$$

being,

$$\sigma^2_{Caillé} = 0.087\eta_{Caillé}D^2_{Lamella} \quad (5)$$

where $\sigma_{Caillé}$ is the mean-square nearest neighbor distance fluctuations, which can give a rough information about the statistical behavior of the interacting bilayers, N is the number of oriented bilayers, and $D_{Lamella}$ is the repeating unit between the lamella. Noteworthy, such methodology is related to the bilayer fluctuation and does not take into account any direct interaction potential. Furthermore, it is important to mention that $\eta_{Caillé}$ is related to the bending modulus, K, and also to the bulk modulus for compression, B, of the lipid bilayers [28,29]. Thus, during the fittings to the experimental data, four other parameters were varied, N, $\sigma_{Caillé}$, $\eta_{Caillé}$ and $D_{Lamella}$, related to the $S(q)$ function on Eqs. (1) and (4). All SAXS data fitting procedure were performed using a Global fitting methodology (GENFIT software), as previously described [31–34].

3. Results and discussion

3.1. Isothermal titration calorimetry

ITC was used in order to evaluate and compare the preference of the $rBPI_{21}$ for different membrane systems. The extension of the interaction was not possible to quantify through a partition model [22,23] due to data quality limitations. However, experimental data were fitted to a "one-site" binding model in order to assess the interaction thermodynamics (Table 1). The calculation of the thermodynamic parameters through this binding model needs to be interpreted with caution, since AMP–membrane interactions are often more complex than a single site binding isotherm [35,36]. POPC:POPG mixtures were used as model systems to mimic the negatively charged membranes of Gram-negative bacteria. On the other hand, the zwitterionic POPC system was used as a model for eukaryotic membranes.

Most of the interactions present a heat flow profile showing an endothermic reaction (Fig. 1). However, in some cases the endothermic interaction is followed by an exothermic reaction after several injections. The presence of the exothermic and endothermic reactions in the same injection for POPC:POPG 30:70, at 15 °C and 25 °C, does not allow the determination of binding parameters accurately from the "one-site" binding model. For that reason, the model was not used for those thermograms (Fig. 1). The thermodynamic parameters obtained by the "one-site" fitting model are shown in Table 1 for POPC:POPG 70:30, 55:45, and 30:70 mixtures. For the remaining lipid mixtures tested, data could not be fitted due to the lack of interaction. A mixture of POPC:POPG 80:20 was also tested, but no heat was developed during the titration (data not shown). The heat production on the $rBPI_{21}$–membrane interaction studies depends on the presence of negatively charged POPG (Fig. 1). On the other hand, for pure POPC bilayers, more similar to eukaryotic membranes, no heat is developed, confirming the absent or weak (undetectable by the instrument) interaction between the AMP and POPC liposomes. Upon the addition of $rBPI_{21}$ to the negatively charged membrane model systems, the heat developed is a sum of several components, namely those associated with $rBPI_{21}$–membrane binding, $rBPI_{21}$–membrane insertion, lipid–lipid aggregation, membrane perturbation, and $rBPI_{21}$ conformational changes [37].

In some cases (POPC:POPG 55:45 and 30:70), both endothermic and exothermic profiles were observed. These complex heat flow profiles have been previously observed for other peptide–lipid interactions. Tritrpticin peptide analogs, Tritrp4 and Tritrp6, have the same profile when interacting with POPE:POPG vesicles [38]. The coexistence of endothermic and exothermic behavior has been considered to be related to other processes, such as pore formation [39], changes in the lipid phase properties during titration [40], or initial peptide aggregation. In order to obtain further information on the interaction between $rBPI_{21}$ and membranes, ITC data was used to calculate the binding isotherm, following the analysis developed by Seelig et al. [35,36]. The binding isotherm is constructed based on the mole fraction of bound AMP per mole of lipid, X_b, at each injection *versus* the equilibrium bulk AMP concentration remaining after each lipid injection, c_f (Fig. 2).

The asymptote represents the maximal AMP interaction with membranes, accounting for the number of AMP molecules bound per lipid in a large excess of the former. If the interaction of the AMP and membrane is entirely hydrophobic in its nature, the relation between X_b and c_f could be expected to be linear, due to a simple partition from aqueous to lipid phase. This would not be true if $rBPI_{21}$ self-aggregates. However, control experiments of $rBPI_{21}$ dilution upon addition of buffer produced only minor heat injections always with the same enthalpy demonstrating the lower tendency for $rBPI_{21}$ to form aggregates in the absence of membranes (data not shown). In relation to the $rBPI_{21}$–membrane interaction, Fig. 2 shows a deviation from linearity. This deviation may be attributed to different effects of $rBPI_{21}$ at the membrane level. Proteins and peptides may induce membrane heterogeneities in the binding site. It is known that POPG may form clusters in the membranes upon positively charged protein or peptide interaction [41]. This eventual negatively charged lipid clustering would condition further protein interactions. It is also possible that the adsorption of the proteins leads to lipid phase separation, which would interfere with the membrane partition of the protein. Thus, during the titrations the overall affinity constant would change.

Table 1
Temperature dependence of the thermodynamic parameters of the binding of $rBPI_{21}$ to LUV of different POPC:POPG mixtures and to LPS, determined by ITC.

	T (°C)	N	ΔH (kcal·mol^{-1})	K_b (M^{-1})	ΔS (cal·mol^{-1}.deg^{-1})	TΔS (kcal·mol^{-1})	ΔG[a] (kcal·mol^{-1})
POPC:POPG 70:30	5	71 ± 10	0.150 ± 0.005	$(7 \pm 1) \times 10^4$	22.6 ± 0.3	6.28 ± 0.08	−6.13 ± 0.07
	15	64 ± 10	0.11 ± 0.01	$(1.7 \pm 0.5) \times 10^5$	24.3 ± 0.6	7.0 ± 0.2	−6.9 ± 0.29
	25	65 ± 10	0.070 ± 0.004	$(6 \pm 3) \times 10^5$	26.6 ± 0.1	7.91 ± 0.02	−7.85 ± 0.02
POPC:POPG 55:45	5	40 ± 7	0.22 ± 0.02	$(7 \pm 1) \times 10^5$	28 ± 1	7.7 ± 0.2	−7.5 ± 0.2
	15	40 ± 5	0.14 ± 0.02	$(2 \pm 1) \times 10^6$	29 ± 1	8. 4 ± 0.4	−8.3 ± 0.4
	25	42 ± 2	0.110 ± 0.009	$(1.4 \pm 0.6) \times 10^6$	28 ± 1	8.5 ± 0.2	−8.4 ± 0.2
POPC:POPG 30:70	5	17 ± 1	0.35 ± 0.05	$(10 \pm 7) \times 10^6$	33 ± 1	9.2 ± 0.3	−8.8 ± 0.4
	15	–	–	–	–	–	–
	25	–	–	–	–	–	–
LPS	5	0.78 ± 0.03	8.5 ± 0.6	$(4.4 \pm 0.2) \times 10^6$	61 ± 1	17.2 ± 0.4	−8.8 ± 0.9
	15	0.83 ± 0.03	5.6 ± 0.4	$(9.88 \pm 0.01) \times 10^6$	51 ± 1	14.6 ± 0.2	−9.0 ± 0.3
	25	0.72 ± 0.02	6.36 ± 0.06	$(8 \pm 2) \times 10^6$	52.8 ± 0.2	15.5 ± 0.2	−9.2 ± 0.2

[a] Free energies were calculated using the equation ΔG = ΔH − T.ΔS.

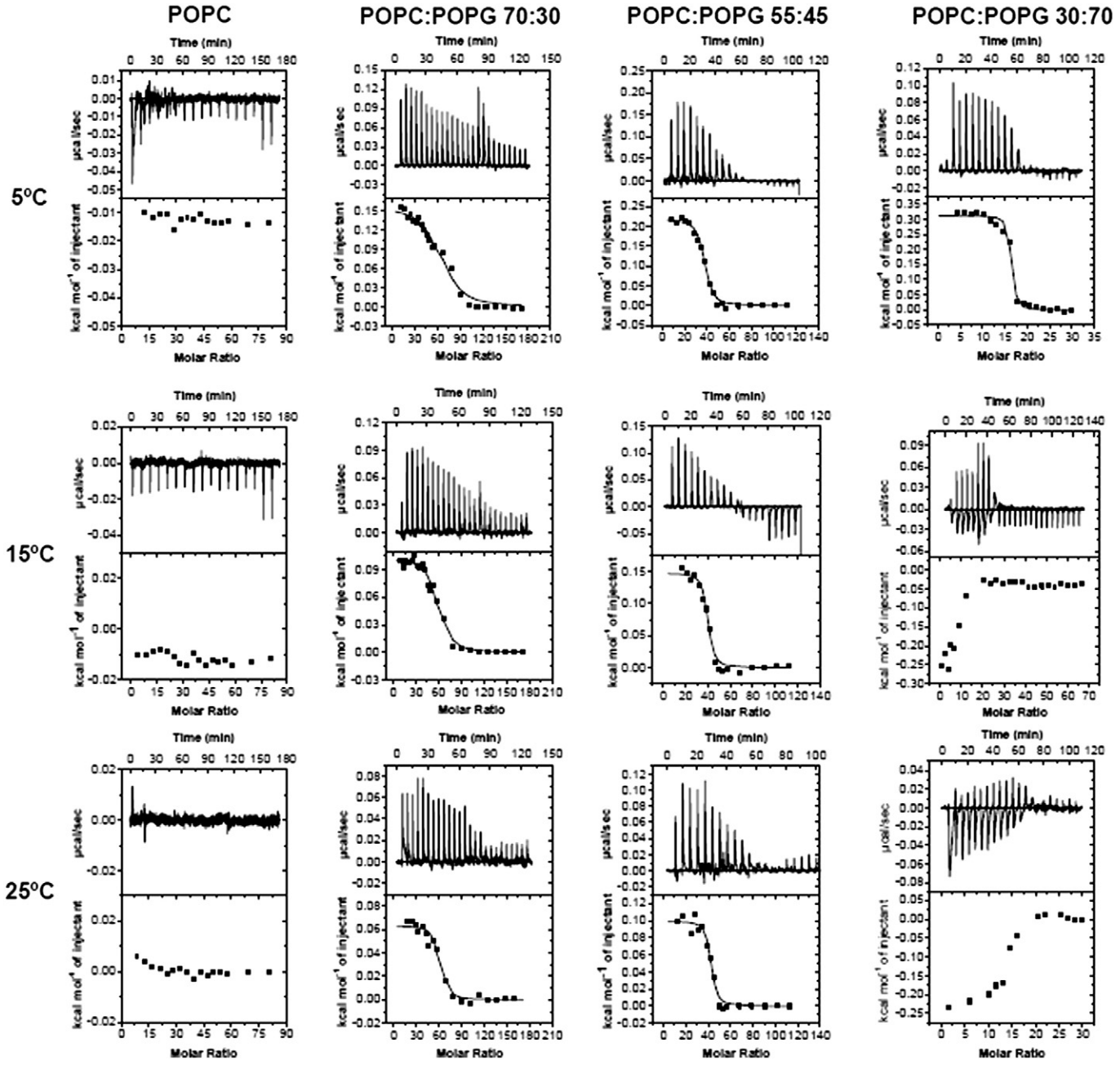

Fig. 1. ITC experimental data (upper graphs) and the heat of injection obtained by integration of the heat flow peaks as a function of the lipid:$rBPI_{21}$ molar ratio (lower graphs), at 5 °C, 15 °C and 25 °C, for POPC and POPC:POPG 70:30, 55:45 and 30:70. In all the sets of measurements, 5 mM lipid suspensions (1 mM for POPC:POPG 30:70) were injected into a 1.4485 mL cell containing 5 μM of $rBPI_{21}$ (for POPC the order of injection was: 5 × 6 μL + 10 × 5 μL + 2 × 15 μL; for POPC:POPG 70:30 and 55:45 it was: 5 × 6 μL + 10 × 5 μL + 5 × 15 μL; and for POPC:POPG 30:70 was: 2 μL + 20 × 10 μL). The same measurements were also conducted for POPC:POPG 80:20. For this case, the heat flow profiles are not shown due to the lack of heat measured during the interaction.

Electrostatic forces may play a major role due to massive AMP:lipid interaction at higher initial peptide concentrations, and the membranes become saturated with the AMP, decreasing the electrostatic attraction. With increasing amounts of lipid, the peptide bulk concentration decreases and there is an equilibrium distribution of $rBPI_{21}$ in the membranes.

The presence of electrostatic interactions or the difference in partition rate toward the different charged vesicles [42] leads to a dependence of the binding constant with the bulk concentration of AMP, through the relation $k_{bc} = X_b/c_f$ (where k_{bc} is the concentration-dependent binding constant) [38]. This phenomenon is observed on the studies of $rBPI_{21}$ interaction with POPC:POPG 70:30 and 55:45, where the isotherms present a curvature. Taking into account that only the external layer of the membrane is exposed for the interaction when calculating X_b, it is evident that the saturation point for POPC:POPG 70:30 changes between 25 and 30 mmol of AMP per mol of lipid, at the temperatures tested. By inverting the values (stoichiometry of the binding of lipid to the AMP), values between 33 and 40 mol of lipid per mol of AMP, for one layer, are obtained. The stoichiometries obtained by the "one-site" binding model (Table 1) for POPC:POPG 70:30 are approximately doubled because the model assumes a bilayer instead of the external exposed layer. This is also true for POPC:POPG 55:45, where the saturation point is achieved when X_b is between 35 and 50 mmol of AMP per mol of lipid, at the temperatures tested. This corresponds to a stoichiometry between 20 and 28 mol of lipid per mol of AMP, assuming only one layer. In this lipid mixture, there

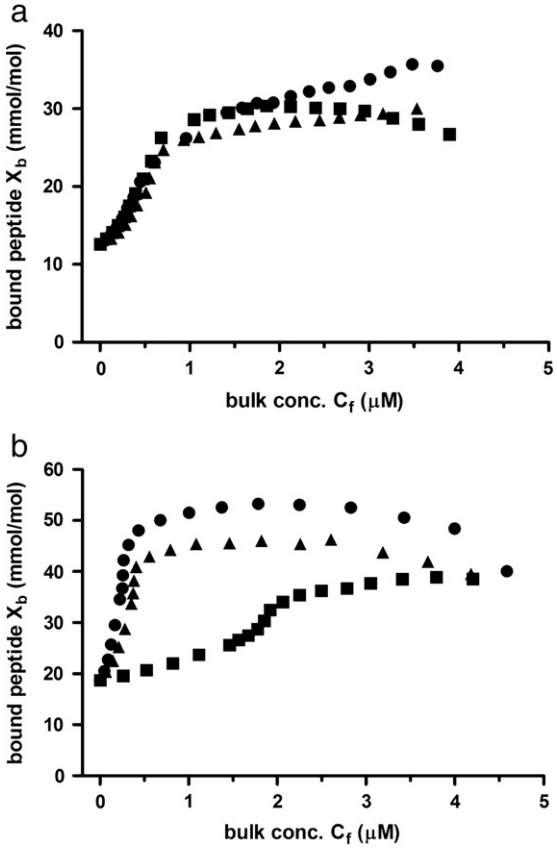

Fig. 2. Binding isotherms calculated from the cumulative heat of reaction of the ITC thermograms of $rBPI_{21}$ binding to membranes of POPC:POPG 70:30 (a) and POPC:POPG 55:45 (b), at 5 °C (circles), 15 °C (triangles) and 25 °C (squares).

is a considerable difference in the saturation point as a function of temperature. At 25 °C, the saturation point is much lower than at 5 °C and 15 °C. The main reason for this may arise from the injection heat produced during the titrations. At 25 °C, for this mixture, the data were very noisy, which may be attributed to other events occurring in the system, eventually associated with membrane perturbations, such as loss of membrane integrity, influencing the binding of $rBPI_{21}$ to lipids.

ITC experiments were also used to study the interaction between $rBPI_{21}$ and LPS, its target molecule in the membrane of Gram-negative bacteria (Fig. 3). An $rBPI_{21}$ solution was titrated with LPS aggregates. The interaction between the AMP and LPS presents a stoichiometry close to 1:1 (Table 1). The heat profile of the interaction is endothermic, suggesting that the binding has a considerable entropic nature. The release of ions from the surface of the LPS might be related to the endothermic profile of the heat flow. In bacterial membranes, LPS is cross-associated by the presence of Ca^{2+} bridging adjacent molecules [43]. One possible component of the mechanism of action of $rBPI_{21}$ *in vivo* may be to induce the release of Ca^{2+} from the bacteria surface, exposing the negative charges of the LPS and its hydrocarbon chains, which may facilitate the permeation of the peptide across the bacterial outer membrane [44]. In the range of temperature tested, the binding is not affected significantly. LPS has a phase transition from a gel-like phase to a fluid phase around 30–37 °C [45]. As LPS maintains its gel-like phase at 5 °C and 15 °C, the interaction is similar for both temperatures. The measurements at 37 °C were extremely noisy and, therefore, they were not completed successfully.

3.2. Differential scanning calorimetry

To further understand $rBPI_{21}$–membrane interaction, we measured by DSC the effect of the peptide in the membrane thermotropic phase transitions of MLV. Two systems were tested: pure DPPC and DPPC:DPPG 55:45, in the presence of different amounts of $rBPI_{21}$ (Fig. 4). Both systems have their highly cooperative main phase transition ($P_{\beta'} \rightarrow L_{\alpha}$) around 41 °C and a pre-transition related to the formation of a ripple phase ($L_{\beta'} \rightarrow P_{\beta'}$) approximately at 33 °C, in accordance with previous reports [46]. For DPPC (Fig. 4a), the membrane structure is not affected by $rBPI_{21}$ up to 20 μM. This result is in agreement with the ITC measurements and previous studies [15,16], where no interaction was observed between the AMP and POPC membranes, showing its weak or absent affinity for zwitterionic membranes. However, with the inclusion of DPPG in the membranes this is altered, as revealed by the thermograms (Fig. 4b). In this

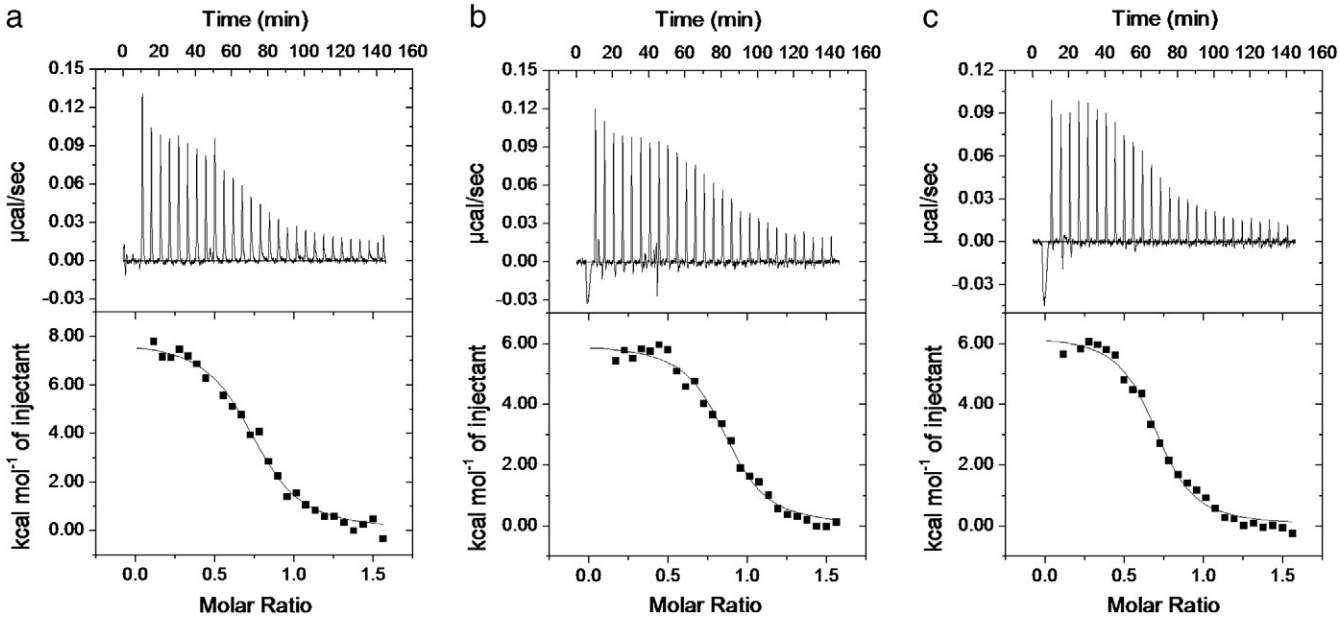

Fig. 3. ITC experimental data (upper graphs) and heat of injection obtained by integration of the heat flow peaks (bottom graphs) for the interaction of $rBPI_{21}$ with LPS aggregates, at 5 °C (a), 15 °C (b) and 25 °C (c). In these experiments, aliquots of 38 μM LPS were injected into a 1.4485 mL cell containing 5 μM $rBPI_{21}$ (the order of injection was: 2 μL + 27 × 10 μL).

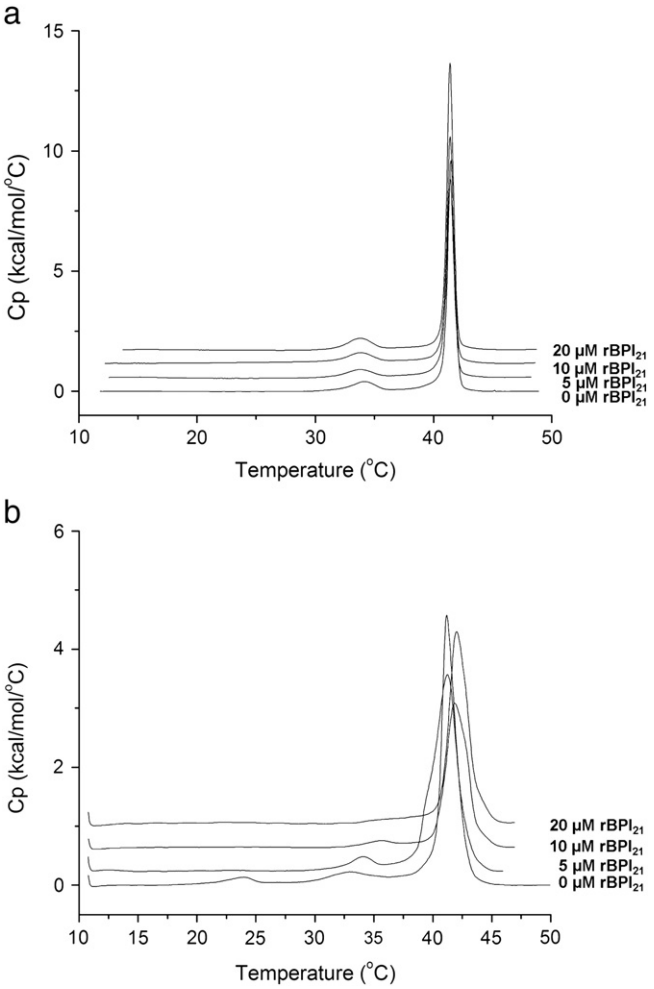

Fig. 4. DSC plots of the gel-to-liquid-crystalline phase transition of DPPC (a) and DPPC:DPPG 55:45 (b), with increasing amounts of $rBPI_{21}$.

mixture, it is also possible to observe two pre-transitions. It could be reasoned that the existence of two pre-transitions may indicate a non-ideal phase coexistence between DPPC and DPPG. Nevertheless, it is described in the literature that DPPC and DPPG tend to mix uniformly at any ratios, with close to ideal behavior, despite the net negative charge of DPPG [47]. The pre-transition at ~23 °C is commonly named subtransition and its molecular details are not very well understood. Due to the time-dependent characteristics of this transition, it is not useful for analytical purposes and, therefore, it was not considered in the analysis [48]. On the other hand, the pre-transition related to the gel to ripple phase formation is useful for analytical considerations, because it is very sensitive to the presence of impurities, such as small molecules and, in this case, the presence of $rBPI_{21}$. By increasing $rBPI_{21}$ concentration, the enthalpy of the pre-transition decreases, while the temperature of the pre-transition increases. At the highest AMP concentration studied, 20 μM, only a shoulder remains in the region of the pre-transition. Furthermore, at this concentration, an increase of 1 °C in the phase transition temperature occurs. The increase in both the pre-transition and main transition temperatures indicates a stabilization of the gel phase ($L_{\beta'}$) upon binding of $rBPI_{21}$. Due to the positive charge of the AMP, the negative charge from DPPG is probably screened, decreasing the electrostatic repulsion between DPPG molecules, ensuring a better packing of the lipid and, consequently, an increase of the van der Waals attraction between lipid molecules, rigidifying the membrane and culminating in a minor increase in the phase transition temperature [46]. Despite the electrostatic screening of DPPG molecules, hydrophobic interaction between hydrocarbon chains and $rBPI_{21}$ can also be related to the increase of the melting temperature of the membrane model system. As seen for a peptide enriched in Leu-Lys amino acid residues [49], the results obtained suggest a possible segregation of lipid domains enriched in PG, promoted by $rBPI_{21}$, culminating in a better packing of PG molecules. Also, the larger effects on the DPPC:DPPG 55:45 system indicate that the negative charge is extremely important for the interaction of $rBPI_{21}$ with membranes, as previously suggested [15,16], correlating with the lower activity in mammalian cells (neutral membranes) while inhibiting bacterial growth (negatively charged membranes).

3.3. Small angle X-ray scattering

Fig. 5a shows the SAXS curves of LUV composed of POPC in the absence and presence of $rBPI_{21}$ 5, 10, and 20 μM. The curves are typical of the scattering from unilamellar vesicles, with a broad peak at $q \sim 0.11$ Å^{-1} [27]. The addition of increasing amounts of $rBPI_{21}$ does not affect significantly the bilayer profile. There is a good fitting of the bilayer structural model (Eqs. (2)−(3); solid lines on Fig. 5a) to the experimental data. The fitting parameters are presented in Table 2 and reveal that the addition of the AMP does not alter the main features of the hydrophobic environment of the zwitterionic membrane. In fact, just a small increase in the polar head thickness from 6.7 Å to 7.2 Å, accompanied by a small decrease in the polar electron density from 0.45 to 0.42 e/Å^3, was observed in the presence of 20 μM $rBPI_{21}$ (Table 2). Therefore, the AMP must reside close to the polar head region of the lipid membrane, without affecting significantly the inner region of the bilayer. This can be correlated with $rBPI_{21}$ weak interaction with the zwitterionic system.

For systems containing the negatively charged lipid POPG, up to three well-defined Bragg peaks appear in the scattering curves when the concentration of the AMP increases, as shown in Fig. 5b–c. This effect is more pronounced when the concentration of the $rBPI_{21}$ reaches 20 μM, where the SAXS curves indeed are typical of the formation of well-ordered MLV [50]. To quantify and better investigate the main features of such structures, the MCT theory was applied to the

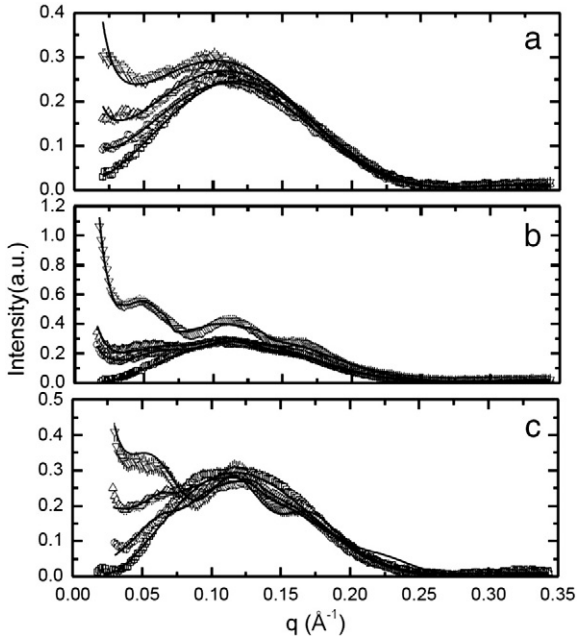

Fig. 5. SAXS curves of POPC:POPG at different molar ratios: 100:0 (a), 80:20 (b) and 55:45 (c). Each system was studied in the absence (squares) and presence of 5 μM (circles), 10 μM (upward triangles) and 20 μM (inverted triangles) of $rBPI_{21}$. All studies were conducted in the presence of 20 mM sodium phosphate buffer pH 7.4, with 150 mM NaCl. Fitting parameters are presented in Table 2.

Table 2
Fitting parameters obtained for the lipid systems composed of POPC or POPC:POPG (80:20 or 55:45) and increasing amounts of $rBPI_{21}$ in 20 mM sodium phosphate buffer pH 7.4, containing 150 mM NaCl. R_{pol}, polar head thickness; R_{par}, acyl chain length; R_{CH3}, methyl length; ρ_{pol}, ρ_{par}, ρ_{CH3}, respective electron densities; $\eta_{Caillé}$, Caillé parameter; N and $D_{Lamella}$, number and average distance of bilayers in one-dimensional lamellar stacking, respectively; $\sigma_{Caillé}$, mean-square nearest neighbor distance fluctuations calculated through Eq. (5); w, weight of MLV contribution to the total scattering (Eq. (1)).

	LUV				MLV			
POPC								
[$rBPI_{21}$] (μM)	0	5	10	20	0	5	10	20
R_{pol} (Å)	6.7 ± 0.3	7.3 ± 0.4	7.1 ± 0.4	7.2 ± 0.4	–	–	–	–
R_{par} (Å)	11.3 ± 0.8	11.3 ± 0.8	11.3 ± 0.8	11.3 ± 0.8	–	–	–	–
R_{CH3} (Å)	3.5 ± 0.2	3.5 ± 0.2	3.5 ± 0.2	3.5 ± 0.2	–	–	–	–
ρ_{pol} (e/Å^3)	0.45 ± 0.01	0.43 ± 0.01	0.43 ± 0.01	0.42 ± 0.01	–	–	–	–
ρ_{par} (e/Å^3)	0.30 ± 0.01	0.30 ± 0.01	0.30 ± 0.01	0.30 ± 0.01	–	–	–	–
ρ_{CH3} (e/Å^3)	0.22 ± 0.01	0.22 ± 0.01	0.22 ± 0.01	0.22 ± 0.01	–	–	–	–
POPC:POPG 80:20								
[$rBPI_{21}$] (μM)	0	5	10	20	0	5	10	20
w (%)						2.0 ± 0.2	3.5 ± 0.4	6.3 ± 0.7
R_{pol} (Å)	9.7 ± 0.8	9.6 ± 0.7	9.5 ± 0.6	8.5 ± 0.7	–	9.6 ± 0.8	9.5 ± 0.6	8.5 ± 0.6
R_{par} (Å)	9.8 ± 0.8	9.8 ± 0.8	9.8 ± 0.8	9.8 ± 0.8	–	9.8 ± 0.8	9.8 ± 0.8	9.8 ± 0.8
R_{CH3} (Å)	3.4 ± 0.2	3.4 ± 0.2	3.4 ± 0.2	3.4 ± 0.2	–	3.4 ± 0.2	3.4 ± 0.2	3.4 ± 0.2
ρ_{pol} (e/Å^3)	0.41 ± 0.01	0.40 ± 0.01	0.40 ± 0.01	0.40 ± 0.01	–	0.40 ± 0.01	0.40 ± 0.01	0.40 ± 0.01
ρ_{par} (e/Å^3)	0.29 ± 0.01	0.29 ± 0.01	0.29 ± 0.01	0.29 ± 0.01	–	0.29 ± 0.01	0.29 ± 0.01	0.29 ± 0.01
ρ_{CH3} (e/Å^3)	0.24 ± 0.01	0.24 ± 0.01	0.24 ± 0.01	0.24 ± 0.01	–	0.24 ± 0.01	0.24 ± 0.01	0.23 ± 0.01
N	–	–	–	–	–	2 ± 1	5 ± 1	7 ± 1
$\eta_{Caillé}$	–	–	–	–	–	0.18 ± 0.02	0.18 ± 0.02	0.18 ± 0.02
$D_{Lamella}$ (Å)	–	–	–	–	–	112 ± 5	112 ± 5	110 ± 5
$\sigma_{Caillé}$ (Å)	–	–	–	–	–	14.0 ± 0.8	14.0 ± 0.8	13.8 ± 0.8
POPC:POPG 55:45								
[$rBPI_{21}$] (μM)	0	5	10	20	0	5	10	20
w (%)						6 ± 1	8 ± 1	12 ± 2
R_{pol} (Å)	9.4 ± 0.6	8.2 ± 0.6	6.5 ± 0.5	6.5 ± 0.5	–	8.2 ± 0.7	6.5 ± 0.6	6.5 ± 0.5
R_{par} (Å)	11.2 ± 0.7	11.2 ± 0.7	12.1 ± 0.7	10.7 ± 0.7	–	11.2 ± 0.5	12.1 ± 0.7	10.7 ± 0.7
R_{CH3} (Å)	3.0	2.8 ± 0.3	2.3 ± 0.2	2.3 ± 0.2	–	2.8 ± 0.3	2.3 ± 0.3	2.3 ± 0.2
ρ_{pol} (e/Å^3)	0.43 ± 0.01	0.39 ± 0.01	0.40 ± 0.01	0.40 ± 0.01	–	0.39 ± 0.01	0.40 ± 0.01	0.40 ± 0.01
ρ_{par} (e/Å^3)	0.31 ± 0.01	0.31 ± 0.01	0.31 ± 0.01	0.31 ± 0.01	–	0.31 ± 0.01	0.31 ± 0.01	0.30 ± 0.01
ρ_{CH3} (e/Å^3)	0.17 ± 0.01	0.18 ± 0.01	0.18 ± 0.01	0.25 ± 0.01	–	0.18 ± 0.01	0.18 ± 0.01	0.25 ± 0.01
N	–	–	–	–	–	3 ± 1	5 ± 1	8 ± 1
$\eta_{Caillé}$	–	–	–	–	–	0.085 ± 0.003	0.085 ± 0.003	0.085 ± 0.003
$D_{Lamella}$ (Å)	–	–	–	–	–	114 ± 5	111 ± 5	107 ± 5
$\sigma_{Caillé}$ (Å)	–	–	–	–	–	9.8 ± 0.6	9.6 ± 0.6	9.2 ± 0.6

data analysis and the percentage of LUV coexisting with MLV was evaluated for each studied membrane composition, using Eq. (1).

The structural parameters of the lipid bilayer composed of POPC:POPG in the absence of $rBPI_{21}$ are very similar to those found in the POPC LUV, except for the polar head thickness that resulted to be *circa* 3 Å-thicker (Table 2). Concerning the POPC:POPG 80:20 membrane, the interaction with $rBPI_{21}$ does not induce any significant change on the lipid bilayer dimensions. Interestingly, the interaction of the peptide with such a membrane containing 20 mol% of negative phospholipids promotes the formation of a small population of MLV coexisting with LUV. In fact, *circa* 2% up to 7% of MLV (w_1 in Eq. (1); Table 2) are formed and contribute to the total scattering intensity when the membrane is in contact with 5 to 20 μM of $rBPI_{21}$, respectively. It should be noted, however, that MLV are composed of a small number of repeating units (up to $N = 7$ for POPC:POPG 80:20 mixed membranes in the presence of 20 μM $rBPI_{21}$; Table 2).

The interaction between $rBPI_{21}$ and POPC:POPG 55:45 membranes causes a decrease in the polar head thickness, with a reduction of the respective polar electron density, as well as a shrinkage in the hydrophobic moiety. Therefore, the thickness of the bilayer containing 45% of negative phospholipids is reduced from 47 ± 2 Å to 40 ± 2 Å when in contact with 20 μM $rBPI_{21}$.

Concomitantly, the percentage of MLV increases for such system in respect to the membrane with a lower amount of POPG, such that the weight of the multilayer scattering to the total scattering intensity, w_1 (Eq. (1), Table 2), increases from 6% to 12% in the presence of 5 and 20 μM of $rBPI_{21}$, respectively. Note, however, that the MLV present a small number of stacking layers, N, too (Table 2). Therefore, the SAXS results give support to the conclusion that the peptide impacts to a larger extent on POPC:POPG 55:45 membranes than it does on POPC:POPG 80:20, in good agreement with ITC and DSC results.

Furthermore, another main difference between the peptide interaction with POPC:POPG 80:20 and 55:45 is reflected in the $\eta_{Caillé}$ value, which decreases as the percentage of anionic lipid increases (Table 2). As a consequence, POPC:POPG 80:20 membranes have a higher $\sigma_{Caillé}$ value (~14.0 Å) than that observed for POPC:POPG 55:45 (~9.5 Å), regardless of the $rBPI_{21}$ concentration (Table 2). Such a result indicates that the interaction between the positively charged AMP and membranes with a higher negative charge reduces membrane fluctuations to a larger extent. This leads to a more rigid membrane, as also observed by DSC.

The number of stacked bilayers, N (Table 2), is independent of the total charge on the membrane surface, being only influenced by $rBPI_{21}$ concentration. For the studied POPC:POPG membranes, 20 μM of the AMP is able to induce the formation of 7 ± 1 multilayers, with a mean distance between two adjacent bilayers, $D_{Lamella}$, of ~108 ± 6 Å (Table 2). Since the lipid bilayer thickness varies between 50 and 40 Å in the absence and presence of the AMP (Table 2), $rBPI_{21}$ must reside between two adjacent bilayers, probably interacting with both charged membrane surfaces. Recently, Trusova et al. [51] studied the effect of lysozyme (a 18 kDa protein) on the morphology of solid-supported lipid bilayers composed of a zwitterionic lipid (PC) in the absence and presence of an anionic lipid (cardiolipin, CL). These authors showed that lysozyme was able to induce the formation of lipid multilamellar stacking, with a $D_{Lamella}$ on the 90–105 Å range. Interestingly, lysozyme and $rBPI_{21}$ have similar molecular weights (18 and 21 kDa, respectively).

In conclusion, $rBPI_{21}$ was shown to be able to interact with membrane model systems when negatively charged phospholipids are present, changing the membrane organization. The interaction is followed by membrane structure alterations, with the AMP promoting the formation of multilamellar arrangements. Taken together, the observations for the interaction of $rBPI_{21}$ with membrane model systems reinforce the proposed mechanism of action of this microbicide agent against Gram-negative bacteria, at the membrane level [15]. In a first step, the peptide seems to be attracted by the negative charge of the LPS to the surface of the bacteria, partitioning to the LPS-rich outer monolayer of the bacteria outer membrane and allowing the peptide to enter in the periplasmic space. There, the negative charges of the phospholipids, both from the inner membrane and from the inner leaflet of the outer membrane (both rich in phosphatidylglycerol) can contribute to the interaction with the peptide. This process would bring together the two membranes of Gram-negative bacteria, inducing their partial or total coalescence, leading to increased permeability, eventual disruption and cell death.

Acknowledgements

$rBPI_{21}$ was a kind gift from XOMA, Ltd. (Berkeley, CA). This work was partially supported by Fundação para a Ciência e a Tecnologia – Ministério do Ensino e Ciência (FCT-MEC, Portugal), by the FP7-PEOPLE IRSES project MEMPEPACROSS (European Union), and by the Brazilian funding agencies Fundação de Amparo à Pesquisa do Estado de São Paulo (FAPESP), Fundação de Amparo à Pesquisa do Estado do Rio de Janeiro (FAPERJ) and Conselho Nacional de Desenvolvimento Científico e Tecnológico (CNPq). MMD acknowledges FCT-MEC PhD fellowship SFRH/BD/41750/2007. RI and LRSBarbosa acknowledge CNPq for research fellowship. The authors are also in debt with Professors Francesco Spinozzi and Paolo Mariani (Università Politecnica delle Marche, Ancona, Italy), who developed and provided the GENFIT software.

References

[1] World Health Organization, http://www.who.int/topics/drug_resistance/en/, (last accessed in February 2012).
[2] R.M. Dawson, C.Q. Liu, Properties and applications of antimicrobial peptides in biodefense against biological warfare threat agents, Crit. Rev. Microbiol. 34 (2008) 89–107.
[3] T. Gura, Innate immunity. Ancient system gets new respect, Science 291 (2001) 2068–2071.
[4] R.E. Hancock, H.G. Sahl, Antimicrobial and host-defense peptides as new anti-infective therapeutic strategies, Nat. Biotechnol. 24 (2006) 1551–1557.
[5] J.M. Boon, B.D. Smith, Chemical control of phospholipid distribution across bilayer membranes, Med. Res. Rev. 22 (2002) 251–281.
[6] R.F. Epand, P.B. Savage, R.M. Epand, Bacterial lipid composition and the antimicrobial efficacy of cationic steroid compounds (Ceragenins), Biochim. Biophys. Acta 1768 (2007) 2500–2509.
[7] K. Matsumoto, J. Kusaka, A. Nishibori, H. Hara, Lipid domains in bacterial membranes, Mol. Microbiol. 61 (2006) 1110–1117.
[8] A.H. Horwitz, S.F. Carroll, R.E. Williams, P.S. Liu, Inclusion of S-sepharose beads in the culture medium significantly improves recovery of secreted $rBPI_{21}$ from transfected CHO-K1 cells, Protein Expr. Purif. 18 (2000) 77–85.
[9] B.J. Appelmelk, Y.Q. An, B.G. Thijs, D.M. MacLaren, J. de Graaff, Recombinant human bactericidal/permeability-increasing protein (rBPI23) is a universal lipopolysaccharide-binding ligand, Infect. Immun. 62 (1994) 3564–3567.
[10] H. Gazzano-Santoro, J.B. Parent, L. Grinna, A. Horwitz, T. Parsons, G. Theofan, P. Elsbach, J. Weiss, P.J. Conlon, High-affinity binding of the bactericidal/permeability-increasing protein and a recombinant amino-terminal fragment to the lipid A region of lipopolysaccharide, Infect. Immun. 60 (1992) 4754–4761.
[11] J.F. Leeuwenberg, M.A. Dentener, W.A. Buurman, Lipopolysaccharide LPS-mediated soluble TNF receptor release and TNF receptor expression by monocytes. Role of CD14, LPS binding protein, and bactericidal/permeability-increasing protein, J. Immunol. 152 (1994) 5070–5076.
[12] R.R. Schumann, Function of lipopolysaccharide (LPS)-binding protein (LBP) and CD14, the receptor for LPS/LBP complexes: a short review, Res. Immunol. 143 (1992) 11–15.
[13] J.E. Parrillo, Pathogenetic mechanisms of septic shock, N. Engl. J. Med. 328 (1993) 1471–1477.
[14] M. Levin, P.A. Quint, B. Goldstein, P. Barton, J.S. Bradley, S.D. Shemie, T. Yeh, S.S. Kim, D.P. Cafaro, P.J. Scannon, B.P. Giroir, Recombinant bactericidal/permeability-increasing protein (rBPI21) as adjunctive treatment for children with severe meningococcal sepsis: a randomised trial, Lancet 356 (2000) 961–967.
[15] M.M. Domingues, M.A.R.B. Castanho, N.C. Santos, $rBPI_{21}$ promotes lipopolysaccharide aggregation and exerts its antimicrobial effects by (hemi)fusion of PG-containing membranes, PLoS One 4 (2009) e8385.
[16] M.M. Domingues, S.C.D.N. Lopes, N.C. Santos, A. Quintas, M.A.R.B. Castanho, Fold–unfold transitions in the selectivity and mechanism of action of the N-terminal fragment of the bactericidal/permeability-increasing protein ($rBPI_{21}$), Biophys. J. 96 (2009) 987–996.
[17] A. Wiese, K. Brandenburg, S.F. Carroll, E.T. Rietschel, U. Seydel, Mechanisms of action of bactericidal/permeability-increasing protein BPI on reconstituted outer membranes of gram-negative bacteria, Biochemistry 36 (1997) 10311–10319.
[18] A. Wiese, K. Brandenburg, B. Lindner, A.B. Schromm, S.F. Carroll, E.T. Rietschel, U. Seydel, Mechanisms of action of the bactericidal/permeability-increasing protein BPI on endotoxin and phospholipid monolayers and aggregates, Biochemistry 36 (1997) 10301–10310.
[19] L.D. Mayer, M.J. Hope, P.R. Cullis, Vesicles of variable sizes produced by a rapid extrusion procedure, Biochim. Biophys. Acta 858 (1986) 161–168.
[20] M.L. Mangoni, R.F. Epand, Y. Rosenfeld, A. Peleg, D. Barra, R.M. Epand, Y. Shai, Lipopolysaccharide, a key molecule involved in the synergism between temporins in inhibiting bacterial growth and in endotoxin neutralization, J. Biol. Chem. 283 (2008) 22907–22917.
[21] E.A. Lewis, K.P. Murphy, Isothermal titration calorimetry, Meth. Mol. Biol. 305 (2005) 1–16.
[22] P.T. Martins, A. Velazquez-Campoy, W.L. Vaz, R.M. Cardoso, J. Valerio, M.J. Moreno, Kinetics and thermodynamics of chlorpromazine interaction with lipid bilayers: effect of charge and cholesterol, J. Am. Chem. Soc. 134 (2012) 4184–4195.
[23] M.J. Moreno, M. Bastos, A. Velazquez-Campoy, Partition of amphiphilic molecules to lipid bilayers by isothermal titration calorimetry, Anal. Biochem. 399 (2010) 44–47.
[24] T. Fruhwirth, G. Fritz, N. Freiberger, O. Glatter, Structure and order in lamellar phases determined by small-angle scattering, J. Appl. Crystallogr. 37 (2004) 703–710.
[25] O. Kratky, G. Porod, The dependence of the X-ray small-angle scattering on shape and size of colloidal particles in solution, Acta Phys. Austriaca 2 (1948) 133–147.
[26] G. Porod, The dependence of the X-ray small-angle scattering on shape and size of colloidal particles in solution, Acta Phys. Austriaca 2 (1948) 252–292.
[27] R.M. Fernandez, K.A. Riske, L.Q. Amaral, R. Itri, M.T. Lamy, Influence of salt on the structure of DMPG studied by SAXS and optical microscopy, Biochim. Biophys. Acta 1778 (2008) 907–916.
[28] A. Caille, Physique cristalline: remargues sur la diffusion des rayons X dans les smectiques, A. C. R. Acad. Sci. Paris. 274 (1972) 891–893.
[29] R. Zhang, R.M. Suter, J.F. Nagle, Theory of the structure factor of lipid bilayers, Phys. Rev. E Stat. Phys. Plasmas Fluids Relat. Interdiscip. Topics 50 (1994) 5047–5060.
[30] R. Zhang, S. Tristram-Nagle, W. Sun, R.L. Headrick, T.C. Irving, R.M. Suter, J.F. Nagle, Small-angle x-ray scattering from lipid bilayers is well described by modified Caille theory but not by paracrystalline theory, Biophys. J. 70 (1996) 349–357.
[31] P. Andreozzi, S.S. Funari, C. La Mesa, P. Mariani, M.G. Ortore, R. Sinibaldi, F. Spinozzi, Multi- to unilamellar transitions in catanionic vesicles, J. Phys. Chem. B 114 (2010) 8056–8060.
[32] L.R. Barbosa, M.G. Ortore, F. Spinozzi, P. Mariani, S. Bernstorff, R. Itri, The importance of protein–protein interactions on the pH-induced conformational changes of bovine serum albumin: a small-angle X-ray scattering study, Biophys. J. 98 (2010) 147–157.
[33] R. Sinibaldi, M.G. Ortore, F. Spinozzi, F. Carsughi, H. Frielinghaus, S. Cinelli, G. Onori, P. Mariani, Preferential hydration of lysozyme in water/glycerol mixtures: a small-angle neutron scattering study, J. Chem. Phys. 126 (2007) 235101.
[34] M.G. Ortore, F. Spinozzi, P. Mariani, A. Paciaroni, L.R. Barbosa, H. Amenitsch, M. Steinhart, J. Ollivier, D. Russo, Combining structure and dynamics: non-denaturing high-pressure effect on lysozyme in solution, J. R. Soc. Interface 6 (Suppl. 5) (2009) S619–S634.
[35] J. Seelig, Titration calorimetry of lipid–peptide interactions, Biochim. Biophys. Acta 1331 (1997) 103–116.
[36] J. Seelig, Thermodynamics of lipid–peptide interactions, Biochim. Biophys. Acta 1666 (2004) 40–50.
[37] T. Abraham, R.N. Lewis, R.S. Hodges, R.N. McElhaney, Isothermal titration calorimetry studies of the binding of a rationally designed analogue of the antimicrobial peptide gramicidin s to phospholipid bilayer membranes, Biochemistry 44 (2005) 2103–2112.
[38] V.V. Andrushchenko, M.H. Aarabi, L.T. Nguyen, E.J. Prenner, H.J. Vogel, Thermodynamics of the interactions of tryptophan-rich cathelicidin antimicrobial peptides with model and natural membranes, Biochim. Biophys. Acta 1778 (2008) 1004–1014.
[39] T. Wieprecht, O. Apostolov, M. Beyermann, J. Seelig, Membrane binding and pore formation of the antibacterial peptide PGLa: thermodynamic and mechanistic aspects, Biochemistry 39 (2000) 442–452.
[40] R.M. Epand, J.P. Segrest, G.M. Anantharamaiah, Thermodynamics of the binding of human apolipoprotein A–I to dimyristoylphosphatidylglycerol, J. Biol. Chem. 265 (1990) 20829–20832.
[41] P. Wadhwani, R.F. Epand, N. Heidenreich, J. Burck, A.S. Ulrich, R.M. Epand, Membrane–active peptides and the clustering of anionic lipids, Biophys. J. 103 (2012) 265–274.
[42] D. Lassiseraye, L. Courtemanche, A. Bergeron, P. Manjunath, M. Lafleur, Binding of bovine seminal plasma protein BSP-A1/-A2 to model membranes: lipid specificity and effect of the temperature, Biochim. Biophys. Acta 1778 (2008) 502–513.
[43] C.R. Raetz, C. Whitfield, Lipopolysaccharide endotoxins, Annu. Rev. Biochem. 71 (2002) 635–700.
[44] S.O. Hagge, M.U. Hammer, A. Wiese, U. Seydel, T. Gutsmann, Calcium adsorption and displacement: characterization of lipid monolayers and their interaction with membrane–active peptides/proteins, BMC Biochem. 7 (2006) 15.

[45] G. D'Errico, A. Silipo, G. Mangiapia, G. Vitiello, A. Radulescu, A. Molinaro, R. Lanzetta, L. Paduano, Characterization of liposomes formed by lipopolysaccharides from Burkholderia cenocepacia, Burkholderia multivorans and Agrobacterium tumefaciens: from the molecular structure to the aggregate architecture, Phys. Chem. Chem. Phys. 12 (2010) 13574–13585.
[46] C. Schwieger, A. Blume, Interaction of poly(L-lysines) with negatively charged membranes: an FT-IR and DSC study, Eur. Biophys. J. 36 (2007) 437–450.
[47] E.J. Findlay, P.G. Barton, Phase behavior of synthetic phosphatidylglycerols and binary mixtures with phosphatidylcholines in the presence and absence of calcium ions, Biochemistry 17 (1978) 2400–2405.
[48] R.L. Biltonen, D. Lichtenberg, The use of differential scanning calorimetry as a tool to characterize liposome preparations, Chem. Phys. Lipids 64 (1993) 129–142.
[49] D.I. Fernandez, M.A. Sani, J.D. Gehman, K.S. Hahm, F. Separovic, Interactions of a synthetic Leu-Lys-rich antimicrobial peptide with phospholipid bilayers, Eur. Biophys. J. 40 (2011) 471–480.
[50] Z. Varga, A. Bota, G. Goerigk, Unbinding transition in lipid multibilayers induced by copper(II) ions, J. Phys. Chem. B 112 (2008) 8430–8433.
[51] V.M. Trusova, G.P. Gorbenko, I. Akopova, J.G. Molotkovsky, I. Gryczynski, J. Borejdo, Z. Gryczynski, Morphological changes of supported lipid bilayers induced by lysozyme: planar domain formation vs. multilayer stacking, Colloids Surf. B: Biointerfaces 80 (2010) 219–226.